6. Coulson, C. A., "Waves," 7 ed., pp. 60-84, Interscience, New York (1955).
7. Handlos, A. E., and Thomas Baron, *A.I.Ch.E. J.*, 3, 127 (1957).
8. "International Critical Tables," Vol. III, p. 254, McGraw-Hill, New York (1928).
9. Kuper, C. G., and P. H. Trevens, *Phys. Soc. Proc.*, 65, 46 (1952).
10. Longuet-Higgins, M. S., *Roy. Soc. London Phil. Trans.*, 245, 535 (1953).
11. Muenz, Kurt, Ph.D. thesis, Univ. Maryland, College Park (1965).
12. ———, and J. M. Marchello, *Rev. Sci. Inst.*, 35, 953 (1964).
13. Schlichting, Hermann, "Boundary Layer Theory," p. 461, McGraw-Hill, New York (1950).
14. Scriven, L. E., *Chem. Eng. Sci.*, 12, 98 (1960).
15. ———, and R. L. Pigford, *A.I.Ch.E. J.*, 4, 439 (1958).
16. Shain, S. A., and J. M. Prausnitz, *ibid.*, 10, 766 (1964).
17. Sternling, C. V., and L. E. Scriven, *ibid.*, 5, 514 (1959).
18. Vivian, J. E., and C. J. King, *ibid.*, 10, 520 (1964).
19. Wehausen, J. V., and E. V. Laitone, "Encyclopedia of Physics," Vol. XX, Springer Verlag, Berlin (1960).

Manuscript received January 27, 1965; revision received September 20, 1965; paper accepted September 20, 1965.

Bubble Motion and Mass Transfer in Non-Newtonian Fluids

STANLEY M. BARNETT, ARTHUR E. HUMPHREY and MITCHELL LITT

University of Pennsylvania, Philadelphia, Pennsylvania

Instantaneous mass transfer coefficients were obtained for the absorption of carbon dioxide bubbles rising in an aqueous solution of sodium carboxymethylcellulose. The rheological character of the solutions was well described by the Ellis model.

Mass transfer coefficients were high initially but trailed off rapidly with bubble age. Exceptions were found at specific diameters where the bubble shape went through a transition. At about 0.2 cm. a transition from ellipsoidal to a sphere shape occurred, which has also been observed in Newtonian fluids. At a larger diameter, however, the non-Newtonian fluid showed a shape change from a spherical "cap" to a "top" shape and finally to an ellipsoid. A sudden increase of mass transfer coefficient accompanied each shape transition.

Drag coefficient data were correlated successfully with a new Reynolds number. The Newtonian and power law portion of the Ellis model each contributed a component to the Reynolds number, which, when added together, correlated drag data for the bubbles as well as for glass spheres.

Attempts to account for transition shape changes and bubble tailing in the non-Newtonian fluid and their effects on bubble mass transfer are included.

This paper covers mass transfer from gas bubbles into a non-Newtonian fluid. Since mass transfer is directly affected by the state of the flow field, for an adequate understanding of the entire operation, it is also necessary to describe the flow conditions. Very little information is presently available. Only recently have theoretical studies of the flow of non-Newtonian fluids over solid spheres (*1, 2*) been published, while even less work has been done on liquid drops, and nothing on gas bubbles. Some results on bubble mechanics and drag in non-Newtonian fluids are also included, since they may provide an insight into the mass transfer phenomena.

Many investigators have studied mass transfer from bubbles in Newtonian systems. For practical reasons most of these studies have concerned themselves with multibubble systems. Those who did work with single bubbles generally obtained their data averaged over the life of a bubble (*3, 4*). In most cases (*5* to *7*), the results were influenced by the wake of a preceding bubble.

Many authors have studied bubble shapes (*8* to *12*). Miyagi (*13*), in particular, provided an excellent study of the shapes and oscillations during a bubble's rise. A comprehensive literature survey may be found in reference *14*.

Deindoerfer and Humphrey (*15*) obtained instantaneous mass transfer coefficients, velocities, and diameters for a bubble rising alone in distilled water. Mundkur (*16*) expanded the range of these data. The technique of Deindoerfer and Humphrey has been criticized in a recent paper by Calderbank and Lochiel (*25*), because bubble volumes and transfer rates were evaluated from projected bubble images and assumed bubble shapes. Calderbank and Lochiel also explained the fact that their data, obtained from a pressure measurement technique, is higher than Humphrey and Deindoerfer's, because the latter may have introduced impurities through the use of a plastic column. This is inferred from the fact that transfer rates decayed most rapidly soon after release, when one would expect the rate of diffusion of impurity to the surface to be highest. It is felt that the latter phenomenon was due not to impurities, but to imperfections in the bubble release mechanism, which allowed wild oscillations of the bubble upon release, giving too high a transfer rate at the outset which quickly decayed to a low value when the

bubble motion became stabilized. In the present work, which uses the method and basic equipment of Deindoerfer and Humphrey, this was not a factor, mainly because of the increased viscosity of the solutions which insured a smooth bubble release. The latter fact also gave more uniform bubble shapes, so that the use of projected images did not, in this case, give rise to any appreciable error.

The instantaneous mass transfer coefficients were obtained according to the method of Deindoerfer (*15*). The instantaneous coefficient is defined by

$$dN/dt = K_L A(C^* - C) \qquad (1)$$

The mass transfer rate can be related to the instantaneous rate of change of bubble volume and position in the column. A few not too restrictive assumptions inherent in this technique are: the gas is pure, except for a small humidification effect; the system is isothermal; the liquid is incompressible and Henry's law applies. The last assumption appears valid for water at the conditions of the experiments. For the present study the same constants were assumed to apply to the aqueous carboxymethylcellulose (CMC) solutions. Also, hydration and ionization effects were neglected (*17*).

With these assumptions, it is easily shown (*15*) that the following expression may be derived for the mass transfer coefficient:

$$K_L = -1/HRT\left[(1/A)\,dV/dt + (V/A)\,[1/(Z + Z_b)]\,dZ/dt\right] \qquad (2)$$

The second term in the brackets arises as a correction to the increasing volume of the bubble due to the decreased liquid head as it rises. With this expression the mass transfer coefficient can be found in terms of easily measurable quantities. If desired, an average coefficient may be calculated by integration.

EXPERIMENTAL

Hercules Powder Company CMC-7HSP carboxymethylcellulose powder was used to prepare the non-Newtonian solutions. The CMC system was chosen because its aqueous solutions behave as pseudoplastic fluids, the solutions are clear and colorless which facilitates visual observation of the bubble, and most properties, especially surface tension, are very close to those of pure water (see Table 1) (*27*). The latter property was of primary importance because of the considerable effect that surface active agents have on mass transfer from bubbles (8). The waterlike properties of this system and the use of carbon dioxide permitted a direct comparison with the results of Deindoerfer and Mundkur.

Table 1. General Properties of an Aqueous CMC-7HSP* Solution

Solution:	C1	C2
Wt. % dry CMC-7HSP:	0.272	0.1055
Density:	1.00 g./cc. at 25°C.	1.00 g./cc. at 25°C.
Surface tension:	74.2 dynes/cm. at 25°C.	72.6 dynes/cm. at 25°C.
Apparent viscosity† at shear rate:		
1.146 sec.$^{-1}$	1.02 poise	0.569 poise
229.0 sec.$^{-1}$	0.432 poise	0.216 poise
Ellis model parameters:		
Φ_0, (sq. cm.)(sec.$^{-1}$)/dyne	0.99	2.45
Φ_1, sec.$^{-1}$ (sq. cm./dyne$^{\alpha}$)	0.73×10^{-2}	0.97×10^{-1}
α, dimensionless	2.13	1.79
Power law parameters:		
n, dimensionless	0.805	0.842
k, (dyne)(sq. cm.)/sec.^{n}	1.385	0.533

* Hercules cellulose gum (sodium carboxymethyl cellulose powder).
† Defined as ratio of stress to rate of shear at given shear rate.

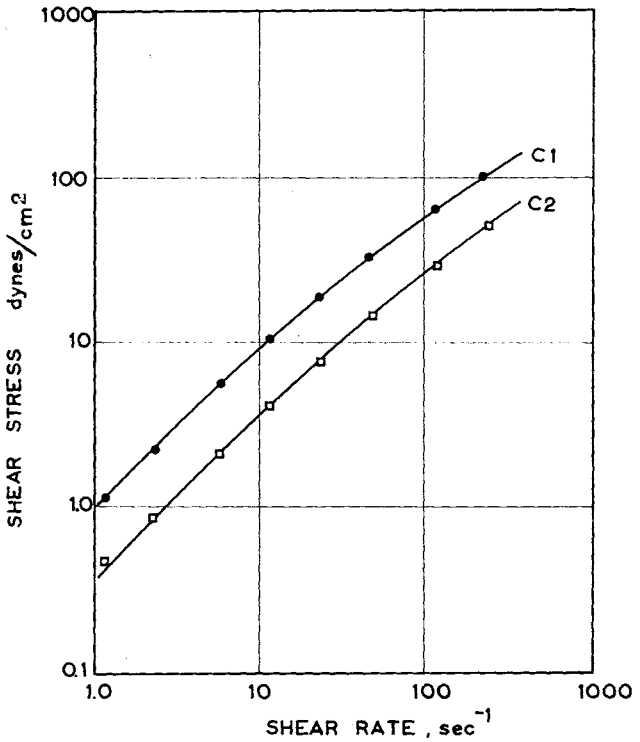

Fig. 1. Shear stress-shear rate curves for CMC solutions.

The solutions were prepared from hot, freshly distilled water and degassed thoroughly before use. All equipment in contact with the solutions and gas was scrupulously cleaned. While surface contamination is always a possibility, it is felt that the careful preparation and degassing procedure should have removed whatever such contamination that was left. Detailed information on solution preparation and cleaning procedures may be found in reference *14*.

A number of solutions of varying CMC concentrations were prepared. Only two, designated C 1 and C 2, were used in the bubble study. A complete description of their properties may be found in Table 1. The rheological properties were determined on a Brookfield synchro-lectric cone-plate viscometer. In addition to determinations made after the solutions were prepared, rheological measurements were repeatedly checked on solutions that were used over any period of time to insure rheological stability of the solutions. Samples kept up to three months showed little or no deterioration (*14*). It is felt that the careful degassing procedure and the use of sterile conditions in the preparation contributed to this stability.

The shear stress–rate-of-strain curves are shown in Figure 1. It was found that the best fit to the curves was given by an Ellis model:

$$\dot{\gamma} = \phi_0\tau + \phi_1\tau^{\alpha} \qquad (3)$$

Values for the Ellis model parameters, as well as power law parameters that were also used, are included.

The equipment consisted of a 150-cm.-long vertical bubble column of 3½ in. sq. cross section. Thirteen interchangeable orifices were used to generate bubbles, ranging from 0.13 to 0.72 cm. in diameter. A Bolex H16 motion picture camera, synchronized with a high intensity lamp, was mounted on a movable platform which was manually raised to follow the bubbles' rise. The photographs of the bubbles were projected to provide enlarged measurements of the major and minor diameter, location, age, and shape. A computer program was written that corrected the measurements for parallax and enlargement and calculated the instantaneous mass transfer coefficient, Reynolds, Sherwood, and Schmidt numbers, and apparent viscosities. The corrected diameter, location, and rise time were plotted to obtain the values for Equation (2) at specified time intervals.

The same procedures, equipment, and solutions were used to determine the drag on carbon dioxide bubbles. In addition,

a separate column was set up to determine the drag coefficients of falling glass spheres to provide a comparison for solid vs. fluid sphere behavior.

The sphere column was a 3⅜ in. diameter glass tube about 48 in. long. Although circular in distinction to the square bubble column, on the basis of approximately equal "diameters," it is felt that wall effects in the two columns should be comparable. A line was drawn on the column about 17½ in. from the tip to mark off the starting point. A second line for the finishing point was drawn 24 in. below the starting mark. A sphere inlet tube, which extended into the solution, was used to dampen initial sphere oscillation due to release.

Glass spheres with a density twice that of water were used. Thus the quantity $(\rho - \rho_s)$ was about the same for both the carbon dioxide bubbles and glass spheres, except, of course, for a sign change. The spheres were selected from "marbles" and beads whose diameter variation for ten readings each was under 1%. Sphere diameters ranged from 0.312 to 1.564 cm.

Before each series of runs, the column was filled with the desired solution and allowed to stand overnight to reach equilibrium conditions. After this stage, a sphere was dropped through the inlet tube and a timer actuated when the particle reached the first mark, and shut off as it passed the second. For the spheres and solutions used, the time of fall was long enough that the error due to starting and stopping the timer was negligible. Also, it was determined that in all cases the spheres achieved terminal velocity prior to reaching the upper mark.

RESULTS

The volume of a dissolving bubble decreases rapidly with time during the early stages and more slowly during the later stages of the bubble's life. Figure 2 shows this effect for both water and the C1 solution for a 3/64 in. orifice. The rate of decrease of volume with time is obviously much slower in the CMC solution than in water, indicating a much slower rate of mass transfer. Primarily, this decreased rate is due to the decreased bubble oscillation in the CMC solution. In water the bubble leaving the orifice would oscillate wildly and spiral as it began its ascent, before it reached a relatively stable shape and rate of rise. In CMC solution this initial period was extremely short or nonexistent.

The mass transfer coefficient showed a similiar decrease with time for run 1, as shown in Figure 3. There was a rather rapid initial decrease corresponding to the rapid initial decrease in bubble volume and then a gradual tapering off. However, in most cases a time was reached in which this trend reversed itself for a short time span and the mass transfer coefficient actually increased with time. This is more strikingly shown for runs 6 and 7. Even though the diameter continues to decrease smoothly, a distinct hump appears in the coefficient curve. The mass

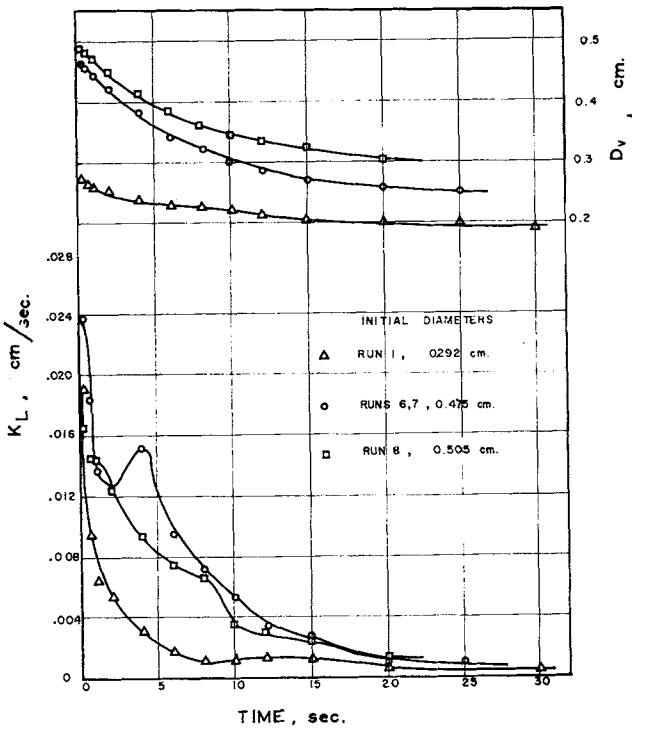

Fig. 3. Instantaneous mass transfer coefficient and bubble diameter vs. time, carbon dioxide in C1 solution.

transfer curve for this run started out as expected, an initial very sharp decrease, but then the trend was reversed. Calculations based on penetration theory do not predict this reversal (*19*), only a continual decrease of the coefficient.

The reason for these humps becomes apparent from a study of curves showing mass transfer coefficient vs. bubble diameter, such as Figures 4 and 5. In Figure 4, for example, peaks in the mass transfer coefficient occur at two diameters, one about 0.2 cm. and the other at about 0.4 cm. More significant is the fact that bubbles starting out at a diameter near one of the peak diameters (such as run 3 in Figure 4) have higher initial coefficients than their neighbors. Run 4 starts at a diameter slightly greater than the peak, so that the initial trend is for its mass transfer coefficient to increase actually with age (or decreasing diameter) until the bubble becomes smaller than the peak diameter. It should always be borne in mind that peak diameter refers to the diameter at which a peak occurs in the mass transfer coefficient; the actual diameter of the

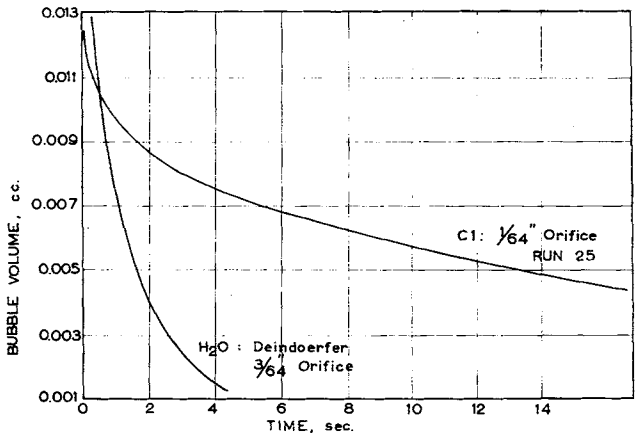

Fig. 2. Volume of carbon dioxide bubble vs. time for water and CMC solution.

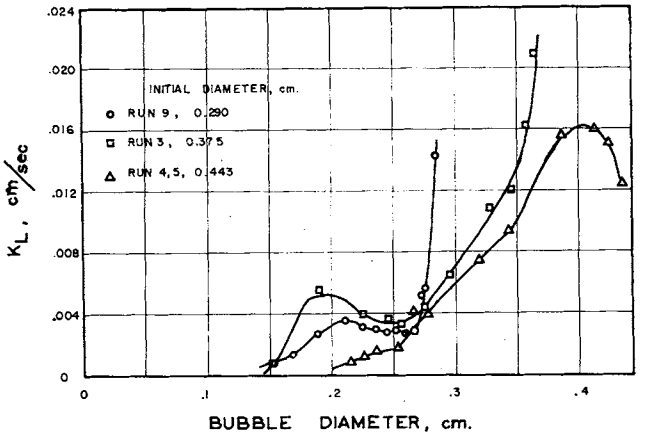

Fig. 4. Instantaneous mass transfer coefficient vs. bubble diameter, carbon dioxide in C1 solution.

bubble is obviously always continuously decreasing, as shown in Figure 3. The runs referred to each represent distinct single bubbles starting from different sized orifices. Those starting from a large size orifice may show both peaks, only the upper peak, or none at all before reaching the top of the column; those introduced from orifices smaller than the upper peak diameter (0.4 cm.) will never show this peak, but may show the lower peak at about 0.2 cm.

The explanation for this seemingly anomalous behavior will become clear from Figure 6 in which K_L for both water and the *C1* solution have been drawn schematically as a function of diameter, with the bubble shape corresponding to each diameter indicated. (The diameter is not the size measured shortly after formation, but at any size after that point. The plot is not to scale.) First, consider the curve for water. As the bubble decreases in size, its shape passes from a "cap" to an ellipsoid and then to a spherical shape. The mass tranfer coefficient meanwhile decreases steadily, mostly due to the decrease in the bubble's oscillatory motion. As the 0.2-cm. diameter point is passed, the coefficient begins to increase, despite the fact that the oscillations are still decreasing. This same region corresponds to the transition from the ellipsoidal to the "solid" sphere region. This shape transition has been mentioned frequently in the literature (*3, 6, 7, 11, 13*). Bubble oscillation alone, however, was considered the cause of the peaks (*7*). In this case, however, the very sharp peaks, and the fact that the experimental photographs clearly show the shape changes at the diameters in question, indicate that these phenomena are due primarily to changes in bubble shape. Some confusion may arise because the diameter change accompanying these transitions may seem small. It must be borne in mind that the "diameter" of the bubbles is calculated from the measured major and minor axes of the projected bubble

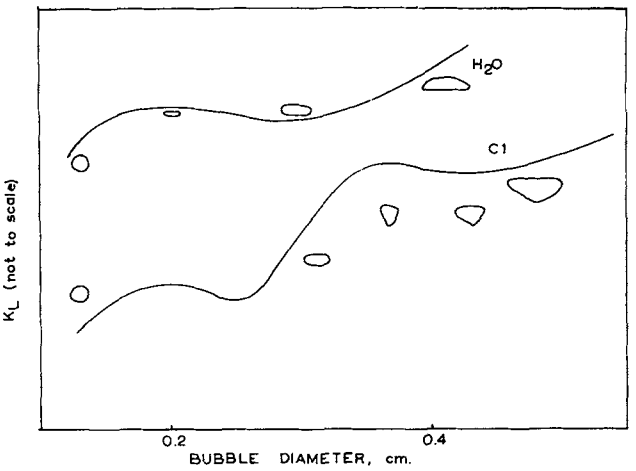

Fig. 6. Schematic drawing of bubble shape changes with diameter.

photograph, assuming an oblate spheroid shape to compute the area and calculating the diameter of the equivalent area sphere. This diameter is relatively insensitive to changes in shape, when the volume is changing only slowly, whereas the mass transfer coefficient, which is strongly influenced by shape and other hydrodynamic factors, will change sharply.

The *C1* curve shows the same phenomenon at 0.2 cm. However, unlike the water curve, there is a second shape transition, producing a second peak in the mass transfer coefficient. The second transition point occurs where the bubble passes from a spherical cap with a tail over to a "top" shape and then to the ellipsoidal shape. The "top" shape occurs over a very narrow range of diameter, which coincides with the peak in the mass transfer coefficient. That the shape transition is due to hydrodynamic rather than mass transfer effect may be concluded from the fact that these same shape changes were also observed with relatively insoluble helium bubbles in these same solutions.

The *C2* solution, being less concentrated, does not show such an abrupt shape change. For this solution, the transition region showed up as a change in the rate of decrease of the minor diameter. This was demonstrated by the fact that the eccentricity of the bubble went through a peak at the same diameter that the mass transfer coefficient did. However, for this less viscous and non-Newtonian solution, the effect was not as marked as for the more concentrated *C1* solution.

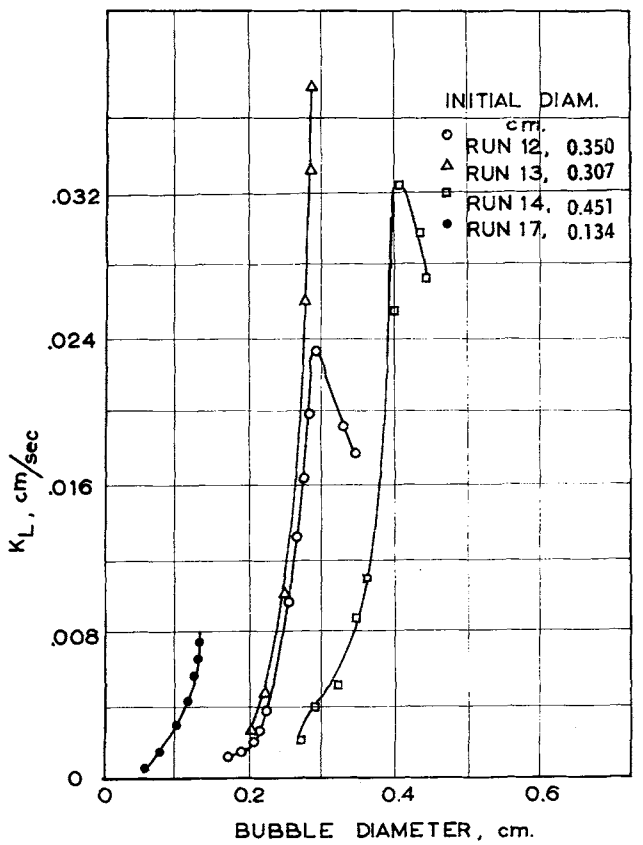

Fig. 5. Instantaneous mass transfer coefficient vs. bubble diameter, carbon dioxide in C2 solution.

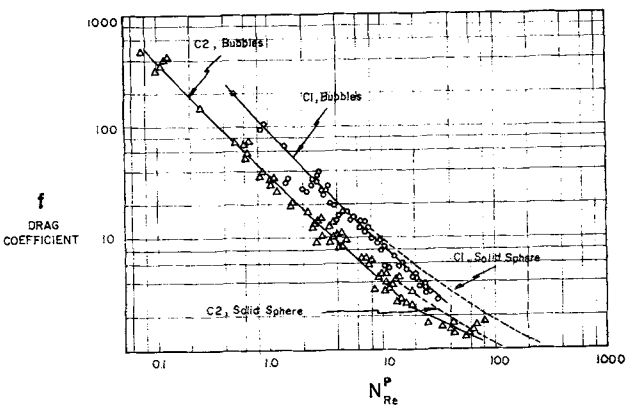

Fig. 7. Instantaneous drag coefficient vs. Reynolds number for power law model, carbon dioxide bubbles in CMC solutions.

In line with the explanation given above, both Deindoerfer (*17*) and Mundkur (*16*) working with water, found only the single transition in the region of 0.2 cm. Indeed, Deindoerfer found that bubbles whose initial diameter was in this region had the highest coefficient for any age bubble, since the shape transition effect was added to the initial, high oscillatory effect to produce a very high rate of mass transfer.

For the non-Newtonian solutions, the coefficients for bubbles originating about the second peak diameter are yet higher. Figure 3 bears out this point for the C1 solution. Runs 6 and 7 start out slightly larger than the second peak diameter and so reach the second peak early in life. These bubbles at all times have a higher mass transfer coefficient than the bubble for run 8, which starts just on the other side of the peak diameter.

For engineering purposes, mass transfer data are often correlated in terms of the dimensionless Sherwood and Peclet numbers. For the present system, the results do not correlate, because the additional parameter of varying bubble shape has not been included. This result is not unexpected, since the available correlations are theoretically based on boundary-layer flow over a nonmobile spherical surface. Any change in the shape or character of the surface, leading to separation, interfacial turbulence, and other changes in the flow pattern, would be expected to produce significant variations in the mass transfer rate.

In an effort to gain more insight into the flow behavior of the bubble, drag measurements were also made. Instantaneous drag coefficients were calculated from diameter and velocity measurements, using the definition for a sphere

$$f = 4/3\ (\rho - \rho_s)/\rho\ gd/U^2 \qquad (4)$$

These data were plotted against two different types of Reynolds numbers for non-Newtonian fluids:

1. Power law fluid: The Reynolds number is usually defined as

$$N_{Re}{}^{P} = \rho \frac{(U)^{2-n}\, d^n}{K\,(3)^{n-1}} \qquad (5)$$

This was used successfully by Fararoui and Kintner (*20*) for correlating data from drops. With the power law parameters for the solutions given in Table 1, the results were plotted as shown in Figure 7. The correlation for each solution is not bad, considering that a power law model does not fit the rheological data too well. Also, the bubble data fall below the solid sphere in each case, indicating that the bubble behaves as a fluid sphere with internal circulation. However, one should expect the curves to converge to a single curve at low Reynolds number, which they do not.

2. Ellis model fluid: Since this model involves three constants, a single dimensionless group cannot correlate the data. Two Reynolds numbers can be derived

$$N_{Re}{}^{0} = \phi_0 U \rho d \qquad N_{Re}{}^{1} = \phi_1 \rho^{a} U^{2a-1} \qquad (6)$$

the first being associated with the Newtonian, and the second with the power law like term of the Ellis model. Slattery (*21*) and Slattery and Bird (*26*)† gave their results

† An error in the definition of Slattery and Bird's parameter B, Equation (35) of reference 26, should be noted. The equation should read

$$B = \phi_0{}^{2a-1}\, \rho^{a-1}\, D^{2(a-1)}/\phi_1$$

The authors are indebted to Professor A. H. P. Skelland for pointing out this correction.

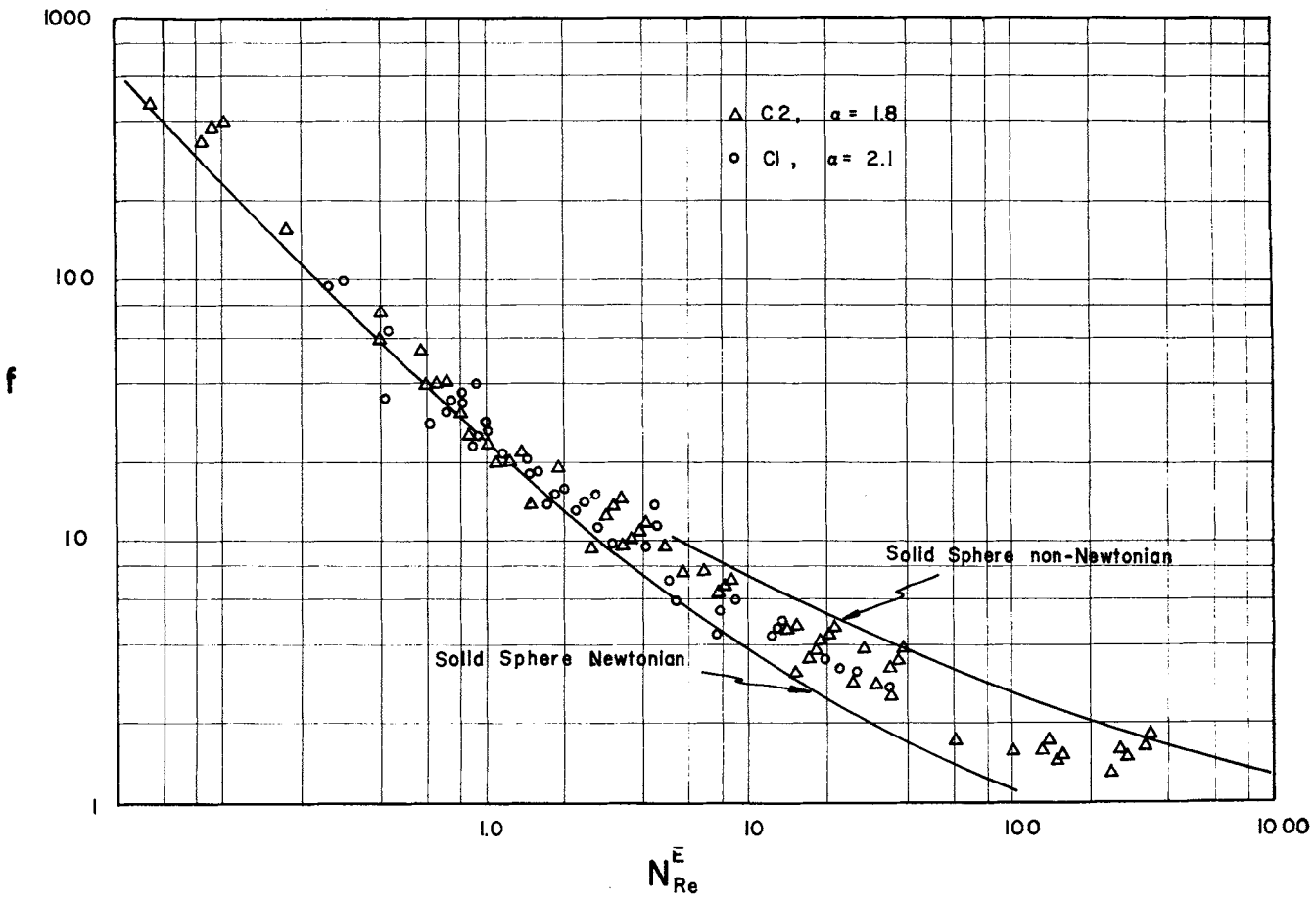

Fig. 8. Instantaneous drag coefficient vs. Reynolds number for Ellis model, carbon dioxide bubbles in CMC solutions.

for sphere drag in CMC solutions, not in terms of the drag coefficient itself, but in terms of a dimensionless correlation for the coefficient f^* which is itself a function of N_{Re}^0, N_{Re}^1, and α. This new parameter f^* is then plotted against N_{Re}^1 and correlates well with the data. Some such type of correlation is required if results are to be plotted vs N_{Re}^1 alone, or significant deviations from expected behavior are found in the low Reynolds number region (*14*).

For the present study, it was decided not to use Slattery and Bird's correlation for two reasons. First, the α for both solutions is greater than the highest value included in the correlation. Indeed, the correlation breaks down for $\alpha > 2$, and that for solution *C2* is 2.13. Second, it was felt to be more convenient to have a single Reynolds number including the effects of both parts of the Ellis model. The simplest combination would be a summation of the two contributions resulting in

$$N_{Re}^E = N_{Re}^0 + N_{Re}^1 \qquad (7)$$

Such a correlation is presented in Figure 8. Besides the original bubble data, the standard Newtonian solid sphere curve and the solid sphere curve for non-Newtonian solutions obtained in this study are included. Again, the bubble data are below the solid sphere data, as in Figure 7, presumably for the same reason. In this case, however, the data approach the Newtonian curve at low Reynolds number, as expected. Also, there is no separation in the data for the two CMC solutions, as obtained with the power law model.

While seemingly there is considerably scatter to the data in Figure 8, it must be remembered that these are instantaneous drag coefficients, not averages taken over timed intervals. In many instances it can be seen that the scatter is not random but seems to have a pattern. This is generally due to the points being for the same bubble. Due to the shape changes discussed above, the drag coefficient also will vary, depending on the initial bubble size and subsequent size history. However, the variation is not as great as with the mass transfer coefficient, and due to the greater uncertainty in the drag coefficient, attempts to construct plots similar to Figures 4 and 5 for the drag coefficient were unsuccessful. Further work with more careful determinations of the instaneous coefficient are needed to tie down this behavior. For Reynolds number less than one, the best fit to the non-Newtonian bubble data is given by

$$f = 28.6/N_{Re}^E \qquad (8)$$

However, the 95% confidence limits are ±40%, so that in this region the data are not significantly different from the Newtonian curve.

Some of the solid sphere data obtained are shown in Figure 9. In addition to the previous two CMC solutions, data are included for a third solution, C3, with $\alpha = 2.3$. Also included are curves for three of Slattery's solutions (*26*) with different values of α. It is apparent that the curves approach the Newtonian line for low Reynolds number. With increasing α, or degree of pseudoplasticity, the drag coefficient increases. This behavior is in qualitative agreement with the calculations of Bizzell and Slat-

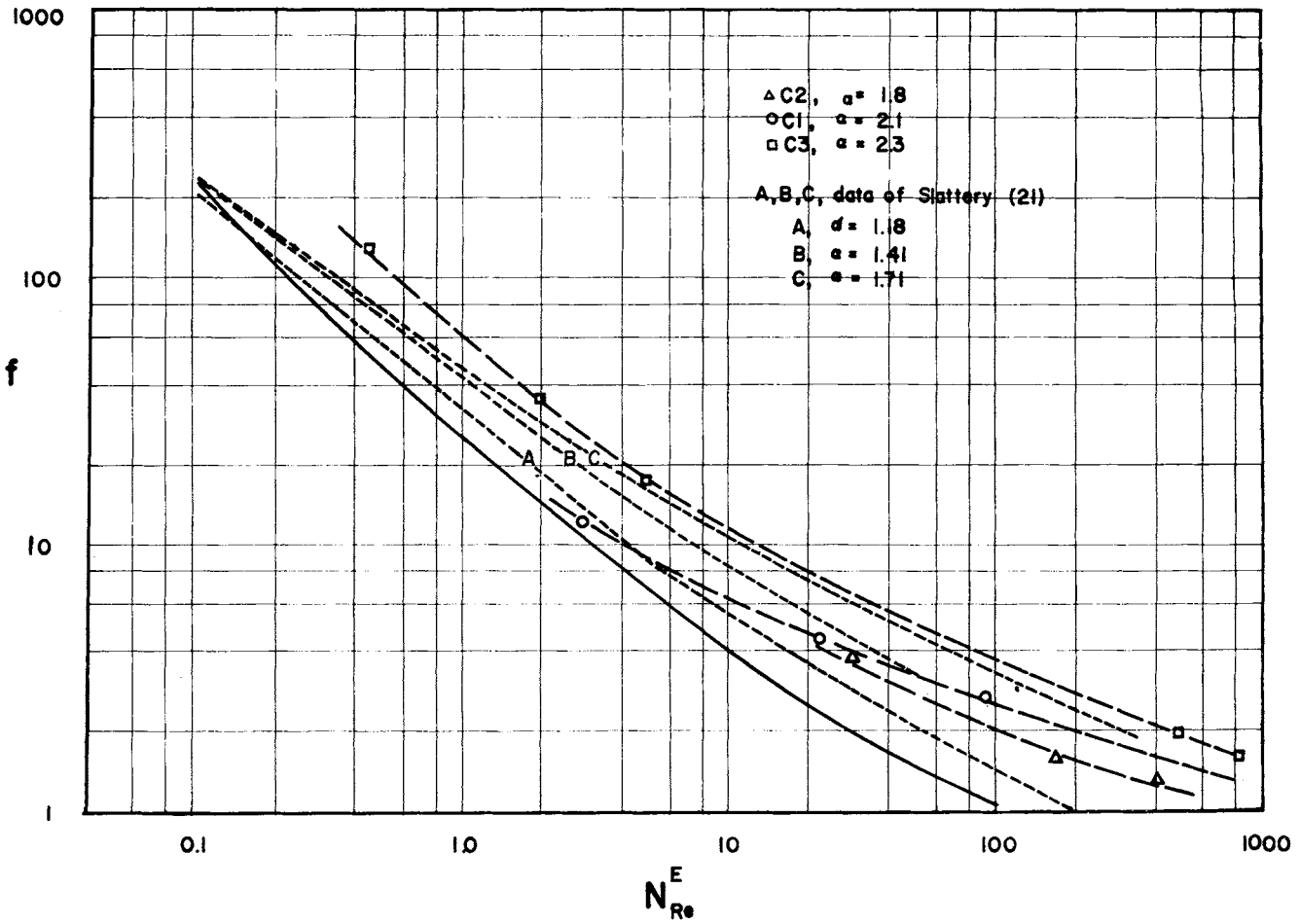

Fig. 9. Average drag coefficient vs. Reynolds number for Ellis model, solid spheres in CMC solutions.

tery (*23*), which show that the separation point should move towards 90 deg. with increasing α, away from the Newtonian case of 83 deg.† However, more extensive data with greater deviation from Newtonian behavior are needed to determine the variation of drag coefficient when the point of separation might be greater than 90 deg.

A possible explanation and interpretation of these phenomena is that the fluid displaced by the bubble's movement fails to recover rapidly enough. The result is a "hole" to the rear of the bubble. This, in turn, sets up an adverse pressure gradient and separation. For a Newtonian fluid, a wake would develop. For a pseudoplastic fluid, however, developing the wake would require more energy than its Newtonian counterpart, slowing down the sphere. If this energy is not supplied, the pressure gradient itself would act as a brake on the sphere. Either condition would result in a greater drag coefficient for the pseudoplastic fluid than for the Newtonian.

This same reasoning would explain the tailing of the bubbles mentioned earlier. This explanation was used by Philipoff (*22*) to explain the tailing of air bubbles in thixotropic solutions. and by Warshay et al. (*24*) to explain the same behavior for liquid drops in CMC solutions. This tailing behavior has been observed only in non-Newtonian fluids. The transition, no doubt, represents the result of a complex interaction of interfacial tension, internal circulation, and other factors. Further experimental work with liquids of varying interfacial tension and different modes of non-Newtonian behavior is necessary to better understand this phenomenon. Thus, the increase in drag coefficient, the second mass transfer coefficient peak, and tailing of the bubble appear to be related to the same hydrodynamic phenomena.

CONCLUSION

Bubble-shape transitions play a dominant role in the mass transfer characteristics of bubbles. The effect of these shape changes becomes more pronounced as the liquid acquires more and more non-Newtonian character. At larger diameters there may be even further shape transitions, giving rise to further anomalous behavior of the mass transfer coefficient.

Drag coefficients of bubbles and glass spheres moving in an Ellis model fluid can be correlated with a new Reynolds number consisting of a summation of the Reynolds number contribution from both the Newtonian and power law like terms of the Ellis model. In the moderate Reynolds number range, the drag coefficient curve for non-Newtonian fluids was higher than the curve for Newtonian behavior.

ACKNOWLEDGMENT

This work was carried out with the support of the National Institutes of Health under U. S. Public Health Service Grant WP-00286.

NOTATION

A = bubble surface area
C = bulk phase concentration
C^* = equilibrium value of carbon dioxide concentration
d = diameter
dN/dt = instantaneous mass transfer rate
f = drag coefficient
K_L = instantaneous mass transfer coefficient
H = Henry's law constant
N_{Re}^{E} = combined Reynolds number, defined by Equation (7)
N_{Re}^{o} = defined by Equation (7)
N_{Re}^{I} = defined by Equation (6) and (7)
N_{Re}^{P} = power law Reynolds number, defined by Equation (5)
R = gas constant
U = velocity
V = instantaneous bubble volume
Z = depth of liquid above bubble's center of gravity
Z_b = atmospheric pressure expressed in height of liquid
α = empirical constant
$\dot{\gamma}$ = rate of shear strain
τ = shear stress
ϕ_0, ϕ_1 = empirical constants
ρ = density
ρ_s = sphere density

LITERATURE CITED

1. Slattery, J. C., *A.I.Ch.E. J.*, **8**, 663 (1962).
2. Wasserman, M. L., and J. C. Slattery, *ibid.*, **10**, 383 (1964).
3. Hammerton, D., and F. H. Garner, *Trans. Inst. Chem. Engrs. (London)*, **32**, 518-524 (1954).
4. Houghton, G., A. M. McClean, and P. D. Ritchie, *Chem. Eng. Sci.*, **7**, 26-39 (1957).
5. Datta, R. L., D. H. Napier, and D. M. Newitt, *Trans. Inst. Chem. Engrs. (London)*, **28**, 14-26 (1950).
6. Guyer, A., and X. Pfister, *Helv. Chim. Acta*, **29**, 1173-1183 (1946).
7. Oyama, Y., and K. Iwase, *Sci. Papers Inst. Phys. Chem. Res. (Tokyo)*, **35**, 131, **36**, 371 (1959).
8. Datta, R. L., *Trans. Indian Inst. Chem. Engrs.*, **14**, 55-57 (1961-62).
9. Ladyzhensky, R. M., *J. Appl. Chem. (U. S. S. R.)*, (Eng. trans.), **29**, 217-224 (1956).
10. *Ibid.*, **27**, 17-25 (1954).
11. Peebles, F. N., and H. J. Garner, *Chem. Eng. Progr.*, **49**, 88-97 (February, 1953).
12. Rosenberg, B., *U. S. Navy Depart. TMB Rept. 727* (September, 1950).
13. Miyagi, O., *Phil. Mag.*, Ser. 6, **50**, 112-140 (1925).
14. Barnett, S. M., Ph.D. thesis, Univ. Pennsylvania, Philadelphia (1963).
15. Deindoerfer, F. H., and A. E. Humphrey, I. E. C., **52**, 755 (1961).
16. Mundkur, S. M., M.S. thesis, Univ. Pennsylvania, Philadelphia (1962).
17. Deindoerfer, F. H., Ph.D. thesis, Univ. Pennsylvania, Philadelphia (1962).
18. Levich, V. G., "Physiochemical Hydrodynamics," 395-472, Prentice-Hall, New York (1963).
19. Bird, R. B. W. E. Stewart, and E. N. Lightfoot, "Transport Phenomena," Wiley, New York (1960).
20. Fararoui, A., and R. C. Kintner, *Trans. Soc. Rheol.*, **5**, 369-380 (1961).
21. Slattery, J. C., Ph.D. thesis, Univ. Wisconsin, Madison (1959).
22. Philippoff, Wladimir, *Rubber Chem. Technol.*, **10**, 76-104 (1937).
23. Bizzell, G. D., and J. C. Slattery, *Chem. Eng. Sci.*, **17**, 777-782 (1962).
24. Warshay, M., E. Bugusz, M. Johnson, and R. C. Kintner, *Can. J. Chem. Eng.*, **37**, 29-36 (1959).
25. Calderbank, P. H., and A. C. Lochiel, *Chem. Eng. Sci.*, **19**, 485 (1964).
26. Slattery, J. C., and R. B. Bird, *ibid.*, **16**, 231 (1961).
27. Bartdorf, J. B., "Industrial Gums," R. L. Whistler, ed., Chapt. 27, Academic Press, New York (1959).

† Professor Slattery has called our attention to an error in reference 23. The last sentence on page 780 should read: These agree qualitatively with available experimental data (*1*) which show the drag coefficient increasing with decreasing $n (n = 1/\alpha$ in (*1*); see also (*15*), suggesting that the point of separation, which experimentally has been observed to be about 83° for a subcritical flow (*16*) moves away from stagnation and toward 90° with decreasing n. 16. Goldstein, S., "Modern Developments in Fluid Mechanics," vol. 2, p. 497, Oxford University Press, 1938.

Manuscript received October 16, 1964; revision received September 30, 1965; paper accepted October 4, 1965. Paper presented at A.I.Ch.E. Memphis meeting